Comparison of 2D and 3D Experiments for IVR

Hae-Kyun Park, Su-Hyeon Kim and Bum-Jin Chung*
Department of Nuclear Engineering, Kyung Hee Univ.,
1732 Deokgyoung-daero, Giheung-gu, Yongin-si, Gyeonggi-do 17104, Republic of Korea
Corresponding author: bjchung@khu.ac.kr

1. Introduction

The integrity of reactor vessel is one of the prime concern in a severe accident condition. When the In-Vessel core melts Retention by External Reactor Vessel Cooling (IVR-ERVC) strategy is adopted as the design concept, the local heat load imposed on the reactor vessel should be identified in order to confirm the integrity of the reactor vessel.

There are several studies [1-8] simulating the natural convection of the oxide pool experimentally. In them, modified Ra (Ra') substitutes conventional Ra in order to represents decay heat of the core melts, due to the self-exothermic condition of the oxide pool. Difficulties in those experiments were the realization of the homogeneous self-exothermic volumetric heat sources. For this reason, the experiments using semicircular facility [1-4] were also carried out instead of those of hemisphere facility [5-8]. The mean and local Nu of the lower head and the top plate were measured and correlations of the mean Nu were developed in existing studies [1, 4, 7-8]. However, the comparisons between 2D and 3D results and phenomenological analyses have not been sufficiently performed.

In this study we measured and compared the mean and local Nu using 2D and 3D Mass Transfer Experimental Rig for Oxide Pool (MassTER-OP). The experiments were carried out using cupric acid copper sulfate (H₂SO₄–CuSO₄) electroplating system based on the analogy between heat and mass transfer system. The Pr was 2,014 and Ra'_H were varied from 7.15×10^{12} to 3.05×10^{15}.

2. Experiments

2.1 Methodology

The analogy between heat and mass transfers was introduced for experimental methodology. Agar [9] figured out that correlations of mass transfer are identical to those of heat transfer under the same conditions. Thus the mass transfer results can substitute the heat transfer results. The analogy of dimensionless number is also established as listed in Table I.

The electroplating system was attempted by Levich [10] for the purpose of conducting the mass transfer experiment firstly. Moreover, Selman *et al.* [11] developed theory of adopting electroplating system under different conditions. The study applied copper sulfate–cupric acid (CuSO₄–H₂SO₄) electroplating system and limiting current technique for experimental performance was used. The current between electrodes is increases as the potential is increases, until the plateau region reaches where the current is stagnant in spite of the potential increase. The plateau section is termed as the limiting current. The cupper ion concentration on the cathode surface is regarded nearly zero. Therefore, mass transfer coefficient (h_m) could be calculated as below:

$$h_m = \frac{(1 - t_{Cu^{2+}})I_{\lim}}{nFC_b} \qquad (1)$$

The mass transfer coefficient (h_m) can be calculated by the bulk concentration (C_b) and the limiting current density ($I_{\lim}$). The total mass-transfer flux is given by I / nF, and the mass-transfer flux by the electric migration is given by $t_{Cu2+} I / nF$. Thus, the mass-transfer flux only by the diffusion and convection phenomena becomes $(1 - t_{Cu2+}) I / nF$. Hence the Sh, calculated by the h_m can substitutes the Nu of the heat transfer system and it is a well-established in previous studies [12-15]. Further details of the experimental method can be found in Ko *et al.* [16].

Table I: Dimensionless numbers for the analogous systems

| Heat transfer		Mass transfer	
Nu	$\dfrac{h_h H}{k}$	Sh	$\dfrac{h_m H}{D_m}$
Pr	$\dfrac{\nu}{\alpha}$	Sc	$\dfrac{\nu}{D_m}$
Ra	$\dfrac{g\beta\Delta T H^3}{\alpha\nu}$	Ra	$\dfrac{gH^3}{D_m\nu}\dfrac{\Delta\rho}{\rho}$

The isothermally cooled boundary conditions have to establish in order to investigate oxide pool by experiment. However, the cathode in terms of the mass transfer experiment has analogy with isothermally heated wall in terms of the heat transfer. Moreover, the limiting current technique is not able to apply for the anode [17]. Thus, the experimental facility of the mass transfer was inverted against the gravity direction for

the purpose of establishing isothermally cooled wall by using limiting current technique.

2.2 Test rig

(a) MassTER-OP2
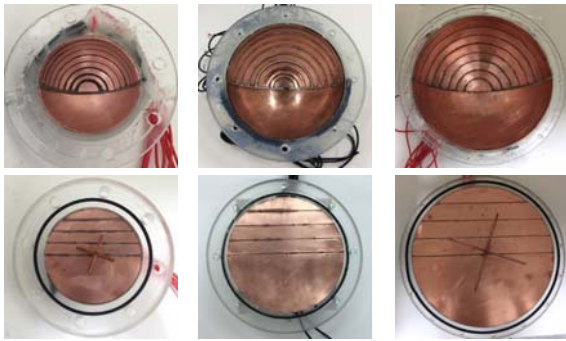
(b) MassTER-OP3

Fig. 1. Photographs of MassTER-OP.

The photographs in Figure 1 present test rigs of the MassTER-OP. All of them were designed with the segments of electrodes in order to measure the local values.

2.3 Test matrix

Table II: Test matrix for MassTER-OP experiments

Test rig dimension	Ra'_H
2D	7.15×10^{12}
	1.74×10^{14}
	1.41×10^{15}
3D	1.81×10^{13}
	4.24×10^{14}
	3.05×10^{15}
$Ra'_H = Ra_H \times Da = \dfrac{g\beta\Delta T H^3}{\alpha v} \times \dfrac{q''H^2}{k\Delta T} = \dfrac{g\beta q'' H^5}{\alpha vk}, Da = \dfrac{q''H^2}{k\Delta T}$	

Table II lists experimental test matrix and the definition of the Ra'_H. The experiments were performed with two and three-dimensional test rig varying three different radii, which results in three different values of

Ra'_H. The isothermal conditions were established on the lower head and top plate during experiment.
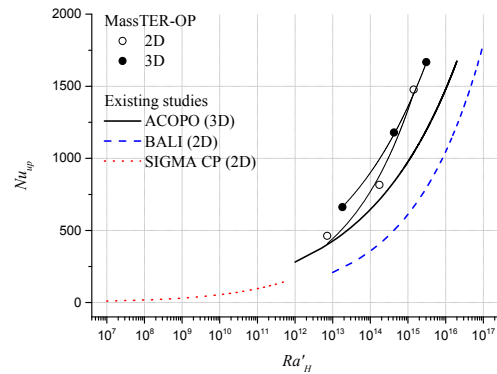
3. Results and discussion

3.1 Measurement validation

The average measurement discrepancies between sum of the piecewises and one-piece electrodes were 4.2% and 7.4%, lower head and top plate respectively. Thus, the piecewise electrodes, which were designed to measure the local value were verified.

3.2 Mean Nusselt numbers
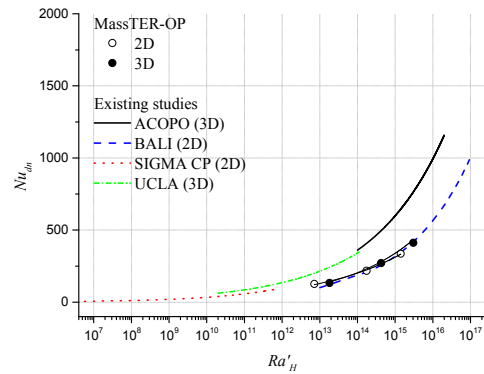
(a) *Nu* of the lower head with respect to the Ra'_H

(b) *Nu* of the top plate with respect to the Ra'_H

Fig. 2. Comparisons of the mean *Nu* between MassTER-OP and existing studies.

Figure 2 shows the mean *Nu*'s of the MassTER-OP and existing studies. The similar trends of *Nu*'s were measured between 2D and 3D results of the MassTER-OP. However, the *Nu*'s of the lower head (Nu_{dn}) were measured about 40% lower than those of the existing studies, while the *Nu*'s of the top plate (Nu_{up}) were measured over 30% higher [18]. The *Nu* correlations with respect to the Ra'_H were developed as below:

$$Nu_{dn3D} = 0.17\, Ra'^{0.22}_H, \qquad (2)$$

$$Nu_{up3D} = 2.81\, Ra'^{0.18}_H, \qquad (3)$$

$$Nu_{dn2D} = 0.43\, Ra'^{0.19}_H,\ \text{and} \qquad (4)$$

$$Nu_{up2D} = 0.34\, Ra'^{0.24}_H. \qquad (5)$$
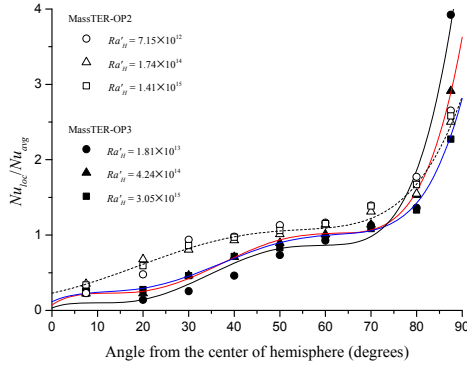
3.3 Local Nusselt numbers

Fig. 3. Comparisons of the angular *Nu* ratios in MassTER-OP.

Figure 3 shows the angular *Nu* ratios (Nu_{loc}/Nu_{avg}) of the MassTER-OP results. The *Nu* ratios increased as the angle increased in all cases. However, the *Nu* ratios of the 2D result measured higher than those of the 3D result at lower angle (20 to 50 degrees). In an IVR condition, the thermal boundary layer of the curvature is developed as angle decreased due to the coolant circulation. However, the width of the semicircular does not changes depending on the angle, while the circumference of the hemisphere changes. Thus, the growth of the boundary layer was accelerated in the hemisphere test rig (3D). Therefore, the higher *Nu* ratios were measured at the lower angle in the 2D experiments than those of the 3D experiments.

The *Nu* ratios of the 2D experiment were independent of the Ra'_H, while those of the 3D experiment in the vicinity of 90 degrees decreased as Ra'_H increased. The flow development, which arises from the bottom to the top edge via top middle were different between 2D and 3D experiments. The one-dimensional flows may be formed in the case of the 2D experiment, due to the fixed width of the semicircular. Meanwhile, the radial flow may be formed at the top middle in the 3D experiment and the increases in radii of the test rig (same as increase in height) would intensify this phenomenon. Thus, the flow velocity nearby the top edge, which enhances the *Nu* ratio of the 90 degrees region in 3D experiments decreased as the Ra'_H increased. The correlations with respect to the lower head angle were expressed as follows:

$$Nu_{Ratio(dn)} = A + B\,\theta + C\,\theta^2 + D\,\theta^3 + E\,\theta^4 + F\,\theta^5.\ (4)$$

Table III: Coefficients of the correlation

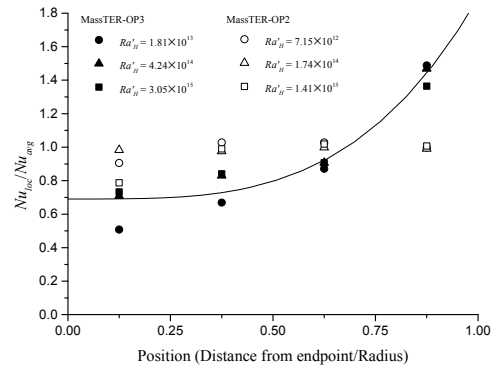| Ra'_H	2D	3D		
	-	10^{13}	10^{14}	10^{15}
A	2.28×10^1	3.23×10^2	7.17×10^2	11.40×10^2
B	1.32×10^2	2.40×10^2	4.12×10^2	2.91×10^2
C	4.02×10^4	-2.97×10^3	-4.00×10^3	-2.61×10^3
D	-1.56×10^6	1.486×10^4	1.672×10^4	1.125×10^4
E	-2.19×10^7	-2.607×10^6	-2.647×10^6	-1.797×10^6
F	2.31×10^9	1.514×10^8	1.423×10^8	9.672×10^9

Fig. 4. Comparisons of the local top plate *Nu* ratios in MassTER-OP.

Figure 4 shows the local top plate *Nu* ratios (Nu_{loc}/Nu_{avg}) of the MassTER-OP results. The almost uniform *Nu* ratios were measured in case of the 2D experiments. Meanwhile, the maximum *Nu* ratios were measured at the top middle and gradually decreased along the flow direction in case of the 3D experiments.

The one-dimensional flows cause the results of 2D experiment. However, the narrow bottom of the lower head concentrates and then accelerates the rise flow in case of the 3D experiments. Therefore, the *Nu* ratio of the top middle was enhanced by the accelerated flow. Then, the radial flow forms from the top middle to the top edge, as explained previously. Thus, the *Nu* ratios of the 3D experiments decreased along the flow direction.

The *Nu* ratios of the top plate showed similar trends regardless of the Ra'_H, while the angular *Nu* ratios were affected in case of the 3D experiments as shown in Fig.3. It seems that the level of contributions to the heat transfer by the flow nearby the top edge is different, between 90 degrees region and the top plate region. The edge flow sweeping the top plate region, collides with the 90 degrees region. Thus, the 90 degrees region was affected by the edge flow rather than the top plate region. And the *Nu* ratio correlations with respect to the position (*R*) of the 3D experiment was developed as below:

$$Nu_{ratio(up)} = 0.69 + 1.20\, Ra'^{3.50}_H. \qquad (7)$$

4. Conclusions

3

The experiments were conducted to simulate oxide pool using mass transfer electroplating system. The 2D and 3D experimental results were compared and the range of the Ra'_H were from 7.15×10^{12} to 3.05×10^{15}.

The similar trends were shown in the mean Nu's between 2D and 3D results, but not for the local Nu's. The angular Nu ratios of the 2D experiments were maximum 2 times higher than those of the 3D experiments at the 20 to 50 degrees. The angular Nu ratio of the 90 degrees region were affected by the Ra'_H in the 3D experiments, while the 2D experiments were not. The local Nu ratios of the top plate measured uniform value in the case of the 2D experiment. However, the maximum Nu ratios of the top plate were measured at the top middle and gradually decreased along the flow direction in the case of the 3D experiments.

It is concluded that the 3D experiment results of the oxide pool could be predicted by conducting the 2D experiment.

ACKNOWLEDGMENT

REFERENCES

[1] J. M. Bonnet and J.M. Seiler, Thermal hydraulic phenomena in corium pools: The BALI experiment, 7th International Conference on Nuclear Engineering, Tokyo, Japan, 1999.

[2] O. Kymalainen, H. Tuomisto, O. Hongisto, T.G. Theofanous, Heat flux distribution from a volumetrically heated pool with high Rayleigh number, Nuclear Engineering and Design, Vol.149, pp.401–408, 1994.

[3] B. R. Sehgal et al., SIMECO Experiments on In-Vessel Melt Pool Formation and Heat Transfer with and without a Metallic Layer, Division of Nuclear Power Safety, Royal Institute of Technology, Brinellvagen 60, 10044 Stockholm, Sweden.

[4] J. K. Lee et al., Experimental study of natural convection heat transfer in a volumetrically heated semicircular pool, Annals of Nuclear Energy, Vol.73, pp.432-440, 2014.

[5] K. Y. Suh et al., In-vessel retention strategy for high power reactors, Korea Electrical Engineering & Science Research Institute, Korea, 2005.

[6] A. Palagin and F. Kretzschmar, LIVE test FSt4: experimental results and simulation by CONV code, The 13th International Topical Meeting on Nuclear Reactor Thermal Hydraulics, Knanazawa City, Japan, 2009.

[7] F.J. Asfia, V.K. Dhir, An experimental study of natural convection in a volumetrically heated spherical pool bounded on top with a rigid wall, Nuclear Engineering and Design, Vol.163, pp.333–348, 1996.

[8] T.G. Theofanous, M. Maguire, S. Angelini, T. Salmassi, The first results from the ACOPO experiment, Nuclear Engineering and Design, Vol.169, pp.49–57, 1997.

[9] N. Agar, Diffusion and convection at electrodes, Discussion of Faraday Society, Vol.26, pp.27-37, 1947.

[10] V. G. Levich, Physicochemical Hydrodynamics, Prentice Hall, Englewood Cliffs & NJ, 1962.

[11] J. R. Selman, et al., Advances in Chemical Engineering, 10th, Academic Press, New York and London, 1978.

[12] B.J. Ko, W.J. Lee, B.J. Chung, Turbulent mixed convection heat transfer experiments in a vertical cylinder using analogy concept, Nuclear Engineering Design, Vol.240, pp.3967-3973, 2010.

[13] J.H. Heo, B.J. Chung, Influence of helical tube dimensions on open channel natural convection heat transfer, International Journal of Heat and Mass Transfer, Vol.55, pp.2829–2834, 2012.

[14] H.K. Park, B.J. Chung, Optimal tip clearance in the laminar forced convection heat transfer of a finned plate in a square duct, International Communications in Heat and Mass Transfer, Vol.63, pp.73–81, 2015.

[15] J.Y. Moon, J.H. Heo, B.J. Chung, Influence of Chimney Widths on Natural Convection Cooling of a Vertical Finned Plate, Nuclear Engineering and Design, Vol.293 pp.503–509, 2015.

[16] S.H. Ko, D.W. Moon, B.J. Chung, Applications of electroplating method for heat transfer studies using analogy concept, Nuclear Engineering and Technology, Vol.38, pp.251–258, 2006.

[17] Y. Konishi et al., Anodic dissolusion phenomena accompanying supersaturation of copper sulfate along a vertical plane copper anode, Electrochimica Acta, Vol.48, pp.2615-2624, 2003.

[18] H. K. Park and B. J. Chung, Mass Transfer Experiments for the Heat Load during In-Vessel Retention of Core Melt, Nuclear Engineering and Technology, (Accepted) DOI information: 10.1016/j.net.2016.02.015.